Dependence of Model-Simulated Heavy Rainfall on the Horizontal Resolution during the Jakarta Flood Event in January−February 2007

Nurjanna J. Trilaksono[1]*, Shigenori Otsuka[1], Shigeo Yoden[1], Kazuo Saito[2], and Syugo Hayashi[2]
[1]*Department of Geophysics, Kyoto University, Kyoto, Japan*
[2]*Meteorological Research Institute, Tsukuba, Japan*

Abstract

Time-lagged ensemble downscaling experiments with Japan Meteorological Agency-Nonhydrostatic model are performed to study the dependence of heavy precipitation simulated by the model on the horizontal resolution for five days during late January to early February 2007, when the Jakarta Flood event occurred. The model runs with horizontal resolutions of 2, 4, and 5 km downscaled from the model runs with a 20-km resolution demonstrate the ability to reproduce a region of strong convective activity to the north of Java Island during the event. Daily meridional propagation of enhanced precipitation signals is simulated in the model runs with 2- and 4-km resolutions.

Cumulative distribution functions of precipitation rate in the model are analyzed for four different regions: ocean, northern coast, mountain, and southern coast. The northern coast region shows the highest contribution of heavy precipitation compared to other regions for all the experiments as well as for satellite-based precipitation estimates. The statistics on the frequency of heavy precipitation show that the diurnal variation of heavy precipitation produced by the model with a 2-km resolution agrees well with that of satellite-based precipitation estimates.

1. Introduction

A tremendous flood event was caused by heavy rainfall that was lasted for several days from late January to early February 2007 in Jakarta and its vicinity. The heavy rainfall is coincided with a strong and persistent trans-equatorial monsoon flow from the Northern Hemisphere (Wu et al. 2007). Trilaksono et al. (2011) investigated spatiotemporal modulation of precipitation and showed that the event associated with a cold surge was preceded by a Borneo vortex event. They also suggested that the convective systems were initiated over the ocean, moved southward, and intensified over the land region, which is consistent with the previous studies that the diurnal variations of precipitation in the tropics have their peaks in the late evening over land regions while in the early morning over adjacent sea regions (e.g., Houze et al. 1981; Mori et al. 2004).

The horizontal resolution of 20 km used in Trilaksono et al. (2011) was insufficient to reproduce the amount of heavy precipitation during the Jakarta Flood event quantitatively. On the contrary, Seko et al. (2008) reported a successful reproduction of an intense rainfall system that developed in Mumbai, India, on 26 July 2005 with horizontal resolutions of 5 and 1 km. Increase of the horizontal resolution was a key factor for the reproduction of heavy rainfall, because the local topography with steep gradients around Mumbai was important for the occurrence.

Although many previous studies conducted high-resolution numerical experiments in the tropics, it is difficult to reproduce the exact location and timing of isolated convections which are generated almost randomly. Probabilistic information from ensemble simulations will be powerful in such a case. But that for the mesoscale convections in the tropics on the time scale of less than a day is not yet studied well.

The diurnal cycle of rainfall is widely known as a prominent feature in the tropical convective systems. To simulate the diurnal cycle realistically, it is necessary to resolve local circulations in association with the land-sea contrast and topographic complexity (e.g., Saito et al. 2001). Because of the existence of spinup processes, ensemble simulations in the tropics may have biases on the diurnal precipitation cycle if all the ensemble members are started from a single local time (Trilaksono et al. 2011). To avoid such a diurnal cycle problem in ensemble simulations, a time-lagged ensemble technique is used in this study.

The purpose of this study is to obtain further understanding of heavy precipitation during the Jakarta Flood event and its reproducibility in the model, including statistical nature of the precipitation. To achieve that, we perform ensemble numerical simulations with different horizontal resolutions. The effects of cumulus parameterizations and local topography are also discussed. To utilize probabilistic information, cumulative distribution functions of hourly precipitation are computed for different regions. Diurnal variations of statistical values are also investigated.

2. Experimental design

Ensemble hindcast experiments with Japan Meteorological Agency-Nonhydrostatic model (JMA-NHM; Saito et al. 2007) are performed from 0000 UTC 31 January to 2300 UTC 4 February 2007. The outer computational domain has 103 × 115 grids with a grid spacing of 20 km, centered at 5°S, 110°E on a Mercator projection. Hereafter, the experiment with this domain is referred to as EXP20km. The subgrid-scale parameterizations and their parameters in EXP20km follow the work by Hayashi et al. (2008) and our previous work (Trilaksono et al. 2011). It employs modified Kain-Fritsch as the cumulus parameterization scheme. We set up three inner domains; they have 250 × 250 grids with a grid spacing of 2 km (the region shown in Fig. 1), 150 × 150 grids with a grid spacing of 4 km, and 120 × 120 grids with a grid spacing of 5 km, centered at northwestern Java. Hereafter, the experiments with these domains are referred to as EXP2km, EXP4km, and EXP5km, respectively. The EXP2km and EXP4km do not use cumulus parameterizations, whereas the EXP5km uses the modified Kain-Fritsch scheme. To avoid undesirable overestimation of the amount of upper-level clouds due to the third-order nonlinear numerical damping, the equivalent 1/e-folding time for the nonlinear numerical damping is increased by 4 times to weaken the nonlinear diffusion (Hayashi 2011).

The National Centers for Environmental Prediction Global Tropospheric Analyses (final analyses) with the horizontal resolution of 1° × 1° and the time interval of six hours are used for the initial and boundary conditions of the EXP20km. The outputs of EXP20km provide the initial and boundary conditions of EXP2km, EXP4km, and EXP5km. The initial data of EXP2km is given by the output of EXP20km at forecast time of 12 hours, whereas for EXP4km and EXP5km initial data are given by that at forecast time of 6 hours. To run the time-lagged ensemble simulation, we follow the same procedure used by Trilaksono et al. (2011). Forecast lengths of EXP2km, EXP4km, EXP5km, and EXP20km for each simulation are 60, 66, 66, and 72 hours,

Corresponding author: Nurjanna J. Trilaksono, Department of Geophysics, Kyoto University, Kyoto 606-8502, Japan. E-mail: jpatiani@kugi.kyoto-u.ac.jp.
*Additional affiliation: Faculty of Earth Sciences and Technology, Institut Teknologi Bandung, Bandung, Indonesia

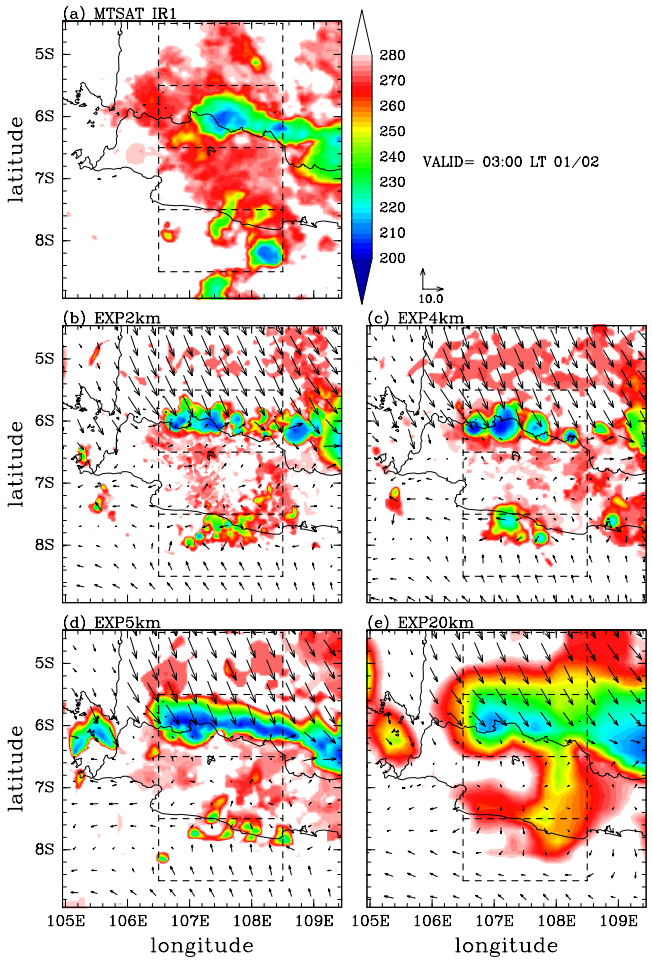

Fig. 1. Horizontal distributions of cloud top temperature (K) of (a) MTSAT IR1 data and a particular ensemble member of (b) EXP2km, (c) EXP4km, (d) EXP5km, and (e) EXP20km at 0300 LT 1 February 2007. Arrows show surface horizontal winds in the models. Unit vectors of 10 m s^{-1} are shown above the panel (c). The four boxes in each plot represent, from north to south, the regions of the ocean, northern coast, mountain, and southern coast. Each box covers an area of 1° × 2° in latitude and longitude.

respectively. Hourly model outputs are analyzed.

To validate the numerical results, we use the Multi-functional Transport Satellite Infrared Channel 1 (MTSAT IR1) data, which is cloud top temperature data for 0.05° × 0.05° grid boxes in every 1 hour and the Tropical Rainfall Measuring Mission (TRMM) 3B42 product (Huffman et al. 2007), which is estimated rainfall data for 0.25° × 0.25° grid boxes in every 3 hours. The analyzed period is five days from 0000 UTC 31 January to 2300 UTC 4 February 2007.

3. Results

3.1 Spatiotemporal distribution of precipitation systems

Figure 1 shows the horizontal distributions of cloud top temperature of (a) MTSAT IR1 data and a particular ensemble member of (b) EXP2km, (c) EXP4km, (d) EXP5km, and (e) EXP20km at 0300 LT (LT denotes local time at Jakarta, UTC +7) 1 February 2007. In Fig. 1a, a zonally elongated strong convective system is observed around 5.6°S−7°S, 107°E−109.5°E. Another region of convective activities is also observed around the southern part of Java Island between 7.2°S−9°S and 107.2°E−108.4°E. Low clouds indicated by temperature of 260−280 K cover more than half of the ocean to the north of Java Island and the inland area, and less than 15% of the ocean to the south of Java Island.

In the model (Figs. 1b−e), the strong convective system observed in Fig. 1a is reproduced well regardless of their horizontal resolutions and cumulus parameterization schemes. The characteristic horizontal scale of deep convection identified by low black body temperature (less than 230 K) of EXP2km is smaller than that of MTSAT IR1, whereas the EXP4km and EXP5km show a comparable scale with that of MTSAT IR1. The EXP5km and EXP20km produce a false convective cell to the west of Java Island, over Sunda Strait (6.2°S, 105.5°E). On the contrary, the EXP2km and EXP4km do not show the appearance of the convective cell over Sunda Strait. All of the model results also reproduce the convective activities around the southern part of Java Island, although their reproducibility are not as good as that in the northern part. The indication of low clouds is identified in all of the model results, even though the result in each resolution shows a different organization of the convective cells. The EXP2km reproduces the low clouds in the inland area between 6.0°S−7.8°S and 106.4°E−108.6°E better than those of the other three.

Figure 1 also shows the surface winds in the models. All the models show a convergence of surface horizontal winds along the northern coast of Java Island (Figs. 1b−e). A relatively weak convergence is also discernible to the south of the island except EXP20km (Figs. 1b−d). These convergence zones correspond to the convective activities to the north and south of the island.

As indicated by dashed lines in Fig. 1, four boxes are introduced to study the contrast of the distribution of precipitation in each region. From north to south, the boxes represent the Java Sea, the northern coast, the mountain region, and the southern coast of Java Island (hereafter referred to as ocean, northern coast, mountain, and southern coast, respectively).

Figure 2 shows the time-latitude cross sections of (a) the TRMM 3B42 estimated precipitation rate and the ensemble mean precipitation rate of (b) EXP2km, (c) EXP4km, (d) EXP5km, and (e) EXP20km averaged between 106.5°E−108.5°E. In the TRMM 3B42 (Fig. 2a), most of the heavy precipitation (≥ 10 mm hr^{-1}) occurs in the northern coast region, not in the other three regions, through the five days. The meridional extent of the heavy precipitation is typically 2° from 5°S−7°S. Midnight enhancement of precipitation is clear in the northern coast region during the five days, and is weakly seen in the southern coast region for the same period except on 4 February.

In all of the model results (Figs. 2b−e), high precipitation rate in the northern coast region is obtained during the five days. The meridional extent of high precipitation rate is about the same or greater than that of TRMM 3B42. Large-scale features in EXP2km, EXP4km, and EXP5km are largely dependent on EXP20km, although we notice some differences from resolution to resolution. Diurnal cycle is clear in all of the model results, whereas in the TRMM 3B42 it is not so clear. Note that passive microwave sensors used in TRMM 3B42 may underestimate precipitation systems that lack the ice phase over land (Huffman et al. 2007). The midnight enhancements of precipitation both in the northern and southern coast regions also appear in all of the model results. The EXP2km and EXP4km show the midnight enhancements of precipitation around 8°S in the southern coast region during the five days, whereas the EXP5km and EXP20km do not show clear enhancements on 2 nor 3 February. Northward propagation of enhanced precipitation signal in the mountain region, which starts around noon, is clear in EXP2km, EXP4km, and EXP5km, particularly on 31 January, 1, and 2 February, whereas in the EXP20km, the propagation is more like north-to-south. Southward propagation of enhanced precipitation signal is also discernible in the ocean region in EXP2km and EXP4km.

3.2 Statistical analyses of heavy precipitation

Figure 3 shows the cumulative distribution functions (CDFs) of precipitation rate of (a) TRMM 3B42, (b) EXP2km, (c) EXP4km, (d) EXP5km, and (e) EXP20km, following the methodology introduced by Trilaksono et al. (2011). These CDFs show the upper tail of the distributions (94−100%) only, as we focus on the heavy rainfall part. To make a direct comparison, we compute two-dimensional running mean of the EXP2km, EXP4km, and

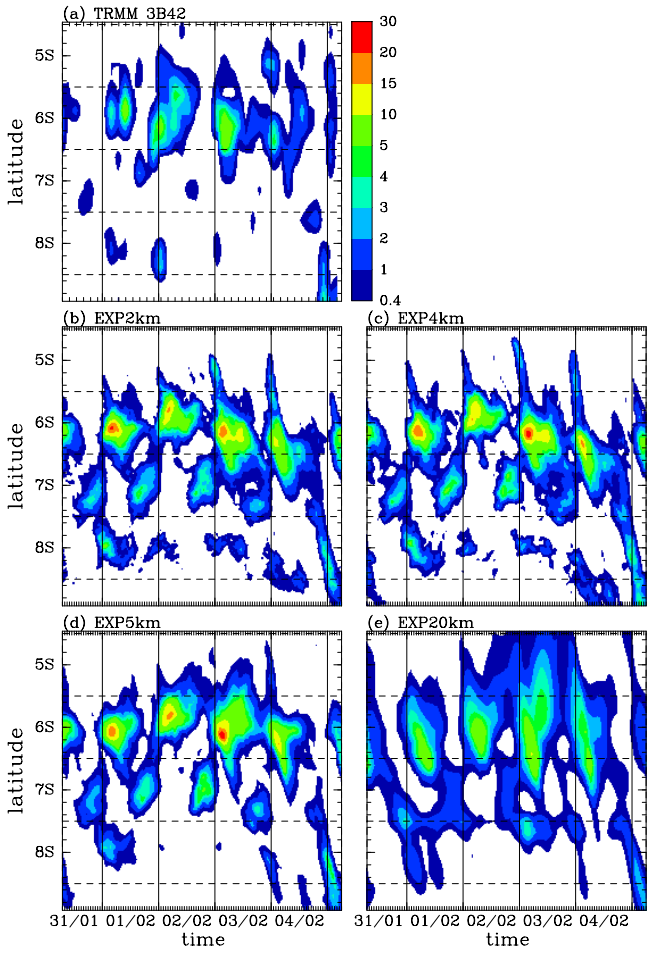

Fig. 2. Time-latitude cross sections of (a) the TRMM 3B42 estimated precipitation rate (mm hr^{-1}) and the ensemble mean precipitation rate (mm hr^{-1}) of (b) EXP2km, (c) EXP4km, (d) EXP5km, and (e) EXP20km from 0700 LT 31 January to 0600 LT 5 February 2007 averaged between 106.5°E−108.5°E. The horizontal dashed lines show the latitudinal boundaries of the four boxes defined in Fig. 1. The vertical lines denote 0000 LT.

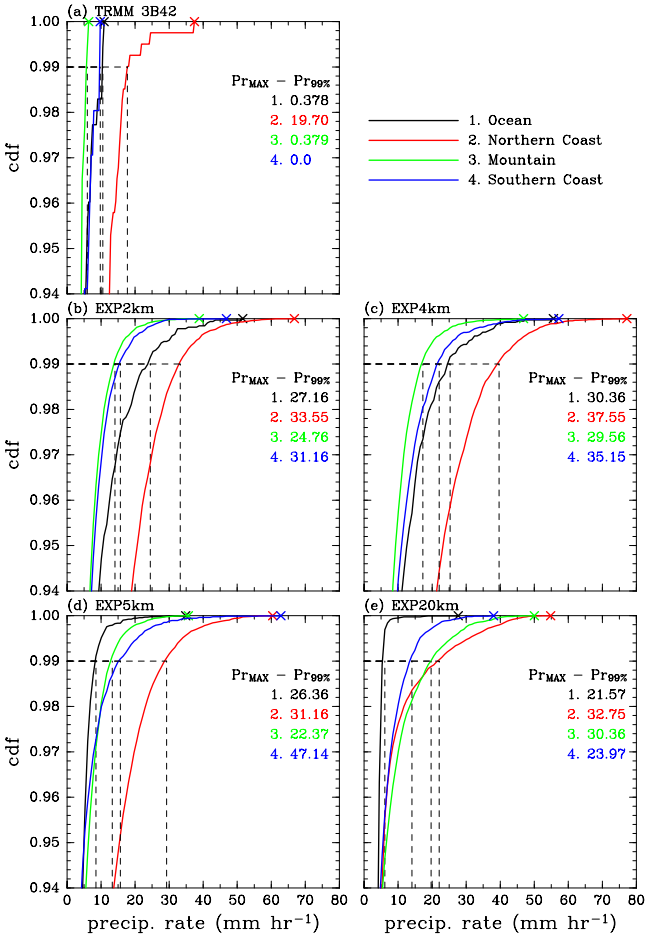

Fig. 3. Cumulative distribution function (CDF) of precipitation rate (mm hr^{-1}) of (a) TRMM 3B42 and all the ensemble members of (b) EXP2km, (c) EXP4km, (d) EXP5km, and (e) EXP20km for the regions of (1) ocean, (2) northern coast, (3) mountain, and (4) southern coast for the five days. The cross symbol denotes the maximum precipitation rate for each region. The vertical and horizontal dashed lines show the intersection point of the 99% of the CDF and the corresponding value of precipitation rate. Numbers in each plot is the maximum precipitation rate minus the precipitation rate at the 99% of the CDF for each region.

EXP5km results with 20 km × 20 km boxes and then interpolate the smoothed data to the EXP20km grids before computing the CDF. In TRMM 3B42 (Fig. 3a), the CDF for the northern coast (red) shows the highest contribution of heavy precipitation to the total amount (over 12 mm hr^{-1} for the top 6%), whereas the lowest one in the mountain region (green) below 10 mm hr^{-1} for 100%. The lack of extreme precipitation especially in the mountain region may be partly due to the limitation of passive microwave sensors over land as noted in the previous subsection.

In the model (Figs. 3b−e), the fact that the northern coast region shows the highest contribution of heavy precipitation is well reproduced except EXP20km, indicating that the downscaling improves the statistical nature of heavy precipitation. The EXP2km and EXP4km (Figs. 3b−c) show the consistent order of the CDF curves for the four regions with that of TRMM 3B42, and the EXP4km shows the highest precipitation rate for the upper tail of the CDF in the northern coast region. The maximum precipitation rate of the EXP4km is 77 mm hr^{-1}. Numbers in each panel show information of very high-end part of CDFs; the maximum value of precipitation rate minus the corresponding value for 99%. In TRMM 3B42, the highest value of this measure is obtained in the northern coast region, and the value is much greater than those in the other regions by a factor of 50 or more, although extreme precipitation over land might be underestimated. Only EXP5km is the exception, in which the highest value is in the southern coast region.

Figure 4 shows the frequency of heavy precipitation as a function of local time for TRMM 3B42 and all the ensemble members of EXP2km over the regions of (a) ocean, (b) northern coast, (c) mountain, and (d) southern coast. The EXP4km shows a similar result, but the EXP2km outperforms the EXP4km in terms of the phase and amplitude of the diurnal variation (not shown). A robust result is obtained using three different thresholds for each dataset: 2, 3, and 4 mm hr^{-1} for TRMM 3B42, and 20, 30, and 40 mm hr^{-1} for the model. In general, the model-simulated diurnal variation of heavy precipitation has qualitatively similar patterns with those of TRMM 3B42. In the northern coast region, where the extreme rainfall probability is the maximum, a broad peak with a minor local minimum extends from 0100 to 1000 LT for TRMM 3B42, whereas in the model, a relatively sharp peak exists at around 0400 LT (Fig. 4b). The midnight peak in the ocean region (Fig. 4a) is a few hours ahead of the peak in the northern coast region, whereas the morning peak in the mountain region in the model (Fig. 4c) is a few hours behind the peak in the northern coast region. This is consistent with the southward propagation of precipitation shown in Fig. 2b, especially on 1, 3, and 4 February, and also consistent with the previous works (e.g., Trilaksono et al. 2011). Although the southward propagation is not clear in TRMM 3B42 due to the limitation of the dataset, the propagation is clear

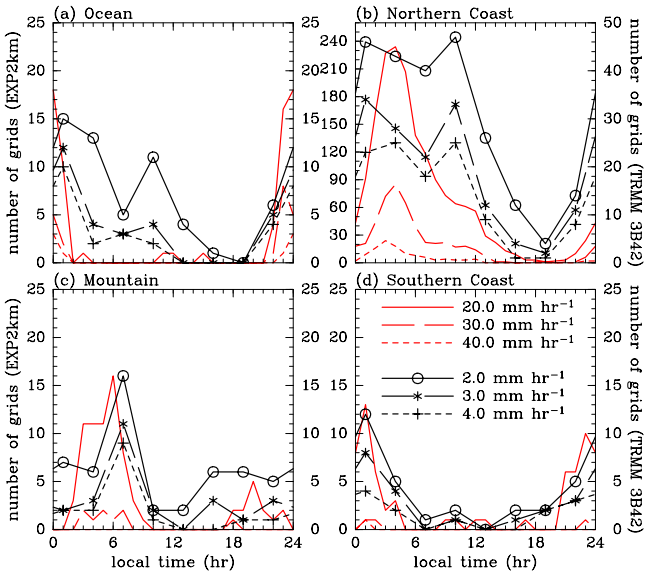

Fig. 4. Frequency of heavy precipitation as a function of local time for TRMM 3B42 (black lines with symbols) and all the ensemble members of EXP2km (red lines) over the regions of (a) ocean, (b) northern coast, (c) mountain, and (d) southern coast. The right y-axis is for TRMM 3B42 and the left y-axis is for EXP2km. The legend inside Fig. 4d shows the threshold values for heavy rainfall, and is used for all the plots in Fig. 4.

in the MTSAT IR1 data (not shown).

4. Concluding remarks

Time-lagged ensemble downscaling experiments with a regional numerical model, JMA-NHM, are performed to study dependence of heavy precipitation on horizontal resolution during the Jakarta Flood event in January−February 2007. The model runs with horizontal resolutions of 2, 4, and 5 km are downscaled from the 20-km runs. The model results demonstrate a good reproducibility of the strong convective system to the north of Java Island at a given time during the flood event as shown in Fig. 1. In particular, the characteristic horizontal scale of deep convections identified from the cloud top temperature in EXP4km and EXP5km is comparable to that of the MTSAT IR1 data, regardless of the adoption of cumulus parameterization. However, the EXP4km shows higher precipitation rates compared to EXP5km (Figs. 3c−d). The differences not only in the maximum value but also in the upper tail of the CDFs suggest that the cumulus parameterization scheme is also responsible for the frequency of heavy precipitation in the model.

Both TRMM 3B42 and the model results show that most of heavy precipitation occurs in the northern coast region that includes Jakarta than the other three regions through the five days (Fig. 4). Daily northward propagation of enhanced precipitation signal starting at around noon in the mountain region is clear in EXP2km, EXP4km, and EXP5km, particularly on 31 January, 1 and 2 February (Fig. 2), presumably due to better representation of complex terrain. The propagation in the mountain region was captured by the X band radar sited at Pondok Betung Meteorological Observatory, Jakarta on 1 and 2 February as shown in Fig. 6 of Wu et al. (2007). Daily southward propagation is also discernible in the ocean region in EXP2km and EXP4km. It is interesting to note that the heavy precipitation in the northern coast region in the first three days occurs at the time when the signals from north and south meet there.

Analysis methods introduced by Trilaksono et al. (2011) are applied in order to reveal statistical nature of heavy precipitation in the downscaling ensemble experiments for the four regions around West Java. The CDFs for the northern coast region show the highest contribution of heavy precipitation to the total amount for both TRMM 3B42 and the model results except EXP20km, demonstrating that the downscaling improves the statistical nature of precipitation (Fig. 3). The diurnal variation of the frequency of heavy precipitation shows a good agreement between TRMM 3B42 and the EXP2km (Fig. 4). In the northern coast region, TRMM 3B42 shows a broad peak of the frequency of heavy precipitation from 0100 to 1000 LT, whereas in the model, a relatively sharp peak exists at around 0400 LT.

In general, the performance of downscaling is good in the situation of Jakarta Flood event in February 2007, in which convective activities play an important role in the heavy precipitation. Finer resolution results show better performance on the precipitation over complex terrain of the mountain region. This is an expedite short report of our first attempt for the specific event, and further investigations with ensemble hindcast datasets are on going in a comprehensive way.

Reference

Hayashi, S., 2011: Statistical verification of short-range forecasts by the NHM and WRF-ARW models with fine resolution. in International Research for Prevention and Mitigation of Meteorological Disasters in Southeast Asia. *Tech. Rep. MRI*, chapter C-2, (in press).

Hayashi, S., K. Aranami, and K. Saito, 2008: Statistical verification of short term NWP by NHM and WRF-ARW with 20 km horizontal resolution around Japan and Southeast Asia. *SOLA*, **4**, 133−136.

Houze, R. A., Jr., S. G. Geotis, F. D. Marks, Jr., and A. K. West, 1981: Winter monsoon convection in the vicinity of north Borneo. Part I: Structure and time variation of the clouds and precipitation. *Mon. Wea. Rev.*, **109**, 1595−1614.

Huffman, G. J., R. F. Adler, D. T. Bolvin, G. Gu, E. J. Nelkin, K. P. Bowman, Y. Hong, E. F. Stocker, and D. B. Wolff, 2007: The TRMM multisatellite precipitation analysis (TMPA): Quasi-global, multiyear, combined-sensor precipitation estimates at fine scales. *J. Hydrometeor.*, **8**, 38−55.

Mori, S., J. Hamada, Y. I. Tauhid, M. D. Yamanaka, N. Okamoto, F. Murata, N. Sakurai, H. Hashiguchi, and T. Sribimawati, 2004: Diurnal land-sea rainfall peak migration over Sumatera Island, Indonesian Maritime Continent, observed by TRMM satellite and intensive rawinsonde soundings. *Mon. Wea. Rev.*, **132**, 2021−2039.

Saito, K., T. Keenan, G. Holland, and K. Puri, 2001: Numerical simulation of the diurnal evolution of tropical island convection over the Maritime Continent. *Mon. Wea. Rev.*, **129**, 378−400.

Saito, K., J. Ishida, K. Aranami, T. Hara, T. Segawa, M. Narita, and Y. Honda, 2007: Nonhydrostatic atmospheric models and operational development at JMA. *J. Meteor. Soc. Japan*, **85B**, 271−304.

Seko, H., S. Hayashi, M. Kunii, and K. Saito, 2008: Structure of the regional heavy rainfall system that occurred in Mumbai, India, on 26 July 2005. *SOLA*, **4**, 129−132.

Trilaksono, N. J., S. Otsuka, and S. Yoden, 2011: A time-lagged ensemble simulation on the modulation of precipitation over West Java in January−February 2007. *Mon. Wea. Rev.*, (in press).

Wu, P., M. Hara, H. Fudeyasu, M. D. Yamanaka, J. Matsumoto, F. Syamsudin, R. Sulistyowati, and Y. S. Djajadihardja, 2007: The impact of trans-equatorial monsoon flow on the formation of repeated torrential rains over Java Island. *SOLA*, **3**, 93−96.

Manuscript received 29 August 2011, accepted 21 November 2011
SOLA: http://www.jstage.jst.go.jp/browse/sola